NJC

PAPER

View Article Online
View Journal | View Issue

Cite this: *New J. Chem.*, 2015, 39, 5293

Synthesis and photoelectric performances of blue-green emitting iridium phenylpyridine complexes using *N*,*N*′-heteroaromatic ancillary ligands†

Xu Huixia,*[ab] Sun Peng,[ab] Zhao Dan,[ab] Yang Tingting,[ab] Hao Yuying,[ac] Wang Hua,[ab] Shi Heping[d] and Xu Bingshe[ab]

Received (in Victoria, Australia) 24th January 2015,
Accepted 13th April 2015

DOI: 10.1039/c5nj00195a

www.rsc.org/njc

Four iridium complexes containing different ancillary ligands Htfmpptz = 2-(5-(4-(trifluoromethyl)phenyl)-2*H*-1,2,4-triazol-3-yl)pyridine, Hfpptz = 2-(5-(4-fluorophenyl)-2*H*-1,2,4-triazol-3-yl)pyridine and Htfmptz = 2-(5-(trifluoromethyl)-2*H*-1,2,4-triazol-3-yl)pyridine and ppy (2-phenylpyridine) as main ligands were synthesized and characterized. Their molecular structures were identified by X-ray single crystal diffraction. The effects of ancillary ligands on the photophysical and luminescence behaviors were investigated. The emission maximum peaks of $(ppy)_2Ir(tfmpptz)$, $(ppy)_2Ir(fpptz)$ and $(ppy)_2Ir(tfmptz)$ in CH_2Cl_2 solution appear at 485, 487 and 483 nm, respectively. Phosphorescent organic light-emitting devices (PhOLEDs) were fabricated using these complexes doped in CBP as an emitting layer.

1. Introduction

Phosphorescent organic light-emitting devices (PhOLEDs) have attracted huge interest due to their high quantum efficiency by utilizing both singlet and triplet excitons.[1–3] Ir(III) complexes, acting as emitters in PhOLEDs, have better performances among numerous metal complexes so far.[4–6] The homoleptic ($Ir(C^N)_3$) and heteroleptic ($Ir(C^N)_2(LX)$) complexes, in which C^N is a cyclometalated ligand and LX is an ancillary ligand, have been developed.[7,8] Since the field strength of an ancillary ligand controls Ir-centered d-(t_{2g}) orbital energy, the singlet metal-to-ligand charge transition (^{1}MLCT) state energy can be tuned by introducing various ancillary ligands without altering the cyclometalate ligand-centered (LC) transition states.[9] And in turn, the emission spectra of $Ir(C^N)_2(LX)$ complexes are changed.[10,11] However, choosing appropriate ancillary ligands to realize blue-light emission still remains an important challenge. It has been demonstrated that the ancillary ligand of *N*,*N*′-heteroaromatic (N^N) has a higher triplet energy level and a lone electron pair of N atoms can regulate effectively the lowest unoccupied molecular orbital (LUMO) levels.[12–15] These complexes with N^N ligands prefer to emit blue and green-blue light.[16–18]

It is well known that tris(2-phenylpyridine)iridium ($Ir(ppy)_3$) is the best green-light emitting material and has excellent electron injection and transport characteristics. In this paper, we will report the blue-green-emitting complexes by introducing the N^N ligands of 2-(5-(4-(trifluoromethyl)phenyl)-2*H*-1,2,4-triazol-3-yl)pyridine (Htfmpptz), 2-(5-(4-fluorophenyl)-2*H*-1,2,4-triazol-3-yl)pyridine (Hfpptz) and 2-(5-(trifluoromethyl)-2*H*-1,2,4-triazol-3-yl)pyridine (Htfmptz) as ancillary ligands into $Ir(ppy)_3$. The molecular structures of all four complexes are described in Scheme 1.

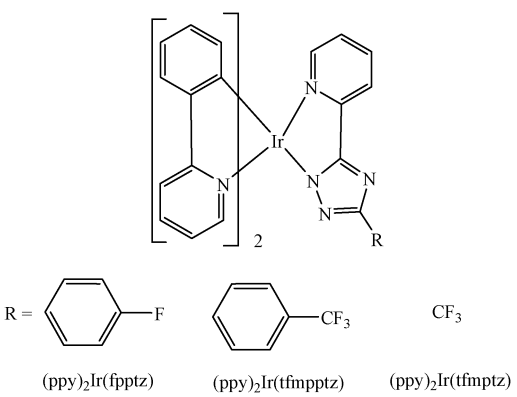

$(ppy)_2Ir(fpptz)$ $(ppy)_2Ir(tfmpptz)$ $(ppy)_2Ir(tfmptz)$

Scheme 1 Molecular structures of $(ppy)_2Ir(fpptz)$, $(ppy)_2Ir(tfmpptz)$ and $(ppy)_2Ir(tfmptz)$.

[a] *Key Laboratory of Interface Science and Engineering in Advanced Materials, Ministry of Education, Taiyuan University of Technology, Taiyuan 030024, P. R. China. E-mail: xuhuixia@tyut.edu.cn; Fax: +86-0351-6010311; Tel: +86-0351-6014852*
[b] *Shanxi Research Center of Advanced Materials Science and Technology, Taiyuan 030024, P. R. China*
[c] *Department of Physics and Optoelectronics, Taiyuan University of Technology, Taiyuan 030024, P. R. China*
[d] *School of Chemistry and Chemical Engineering Shanxi University, Taiyuan 03006, P. R. China*

† CCDC 905311, 905312 and 905314. For crystallographic data in CIF or other electronic format see DOI: 10.1039/c5nj00195a

2. Experimental section

2.1 General information

X-ray single-crystal diffraction of all complexes was performed on a Bruker SMART APEX II diffractometer with Mo Kα radiation (λ = 0.710 73 Å). The structures were solved using direct methods (SHELX-97) and refined using the full-matrix least-squares technique. All non-hydrogen atoms were refined anistropically and hydrogen atoms of organic ligands were geometrically placed.

All calculations were performed using the Gaussian 03 package by employing experimental parameters determined by X-ray single-crystal diffraction as an input file. The geometry optimization of the ground state by density functional theory (DFT) was carried out using the B3LYP functional with 6-31G(d) basis sets,[19,20] except for LANL2DZ basis sets for Ir atoms.

^{1}H NMR data were recorded using a Bruker 600 MHz spectrometer. FT-IR spectra were recorded using a Nicolet 7199B spectrometer in KBr pellets in the range of 4000–400 cm^{-1}. Elemental analyses of carbon, hydrogen, and nitrogen were performed using a Vario EL microanalyzer. UV-vis absorption spectra were recorded using a Lambda Bio 40. The fluorescence spectra were examined using a HORIBA FluouoMax-4 spectrophotometer in dichloromethane (CH_2Cl_2) solution. The absolute fluorescence quantum yields of solution (2×10^{-5} mol l^{-1}) were measured using a HORIBA FluouoMax-4 equipped with an integrating sphere. Cyclic voltammetry was performed using an Autolab/PG STAT302 in a one-compartment electrolysis cell using two platinum wires as a working electrode and a counter electrode, and a calomel electrode as reference. $TBAPF_6$ was used as a supporting electrolyte (0.1 M). Cyclic voltammetric behaviors were monitored at a scan rate of 50 mV s^{-1}.

Organic layers were fabricated by high-vacuum (3×10^{-4} Pa) thermal evaporation onto a glass substrate precoated with an ITO (indium tin oxide) layer. The device structures were ITO/NPB (40 nm)/CBP: $(ppy)_2Ir(N^\wedge N)$ (6 wt%, 30 nm)/TPBi (35 nm)/LiF(1 nm)/Al (200 nm). Materials used for the device are NPB (*N*,*N*′-bis(naphthalen)-*N*,*N*′-bis(phenyl)-benzidine) as a hole-transport layer, Ir(III) complexes (6 wt%) in CBP (4,4′-*N*,*N*′-dicarbazole-biphenyl) as an emitting layer, and TPBi (2,2′,2″-(1,3,5-phenylene)-tris-(1-phenyl-1*H*-benzimidazole)) as an electron-transport layer. The electroluminescence (EL) spectra were recorded using a PR-655 spectrofluorometer. The luminance–voltage–current density (*V*–*L*–*J*) and current efficiency–current density–power efficiency (η_c–*J*–η_p) characteristics of PhOLEDs were recorded on a Keithley 2400 Source Meter and an L-2188 spot Brightness Meter.

2.2 Synthesis of complexes

Solvents for chemical synthesis were purified according to the standard procedures. All reactions were carried out under a dry and oxygen-free atmosphere. The N^N ligands of Htfmpptz, Hfpptz and Htfmptz were synthesized according to ref. 15. 2-Phenylpyridine (H ppy) and iridium trichloride hydrate in 2-ethoxyethanol and water (3 : 1) solution were treated to obtain the chloride-bridged dimer $[(ppy)_2Ir(\mu\text{-}Cl)_2]$ according to the literature procedure.[21]

Complex $(ppy)_2Ir(tfmpptz)$. $(ppy)_2Ir(\mu\text{-}Cl)_2$, K_2CO_3 and the Htfmpptz ligands (2 : 1 : 20) were added in 2-ethoxyethanol (25 ml) at 140 °C for 24 h. After cooling to room temperature, the mixture was poured into water for extraction. The residue was dried in a vacuum for 12 h and then recrystallized from methanol/acetonitrile/dichloromethane (1 : 3 : 30) to obtain the $(ppy)_2Ir(tfmpptz)$ complex in a yield of 65%. ^{1}H NMR (600 MHz, DMSO-d_6): δ 8.22 (1H, s), 8.20 (1H, s), 8.19 (1H, d), 8.15 (1H, s), 8.14 (1H, s), 8.06 (1H dt), 7.89–7.82 (3H, m), 7.83 (1H, d), 7.71 (1H, s), 7.70 (1H,s), 7.65 (2H, dd), 7.62 (1H, d), 7.40 (1H, ddd), 7.20 (1H, ddd), 7.15 (1H, ddd), 6.97 (1H, dt), 6.90 (1H, dt), 6.88 (1H,dt), 6.78 (2H, dt). FT-IR (KBr) cm^{-1}: 2025, 1644, 1611, 1478, 1420, 1324, 1167, 1121, 1063, 868, 764, 727, 503. Anal. calcd for $C_{36}H_{24}F_3IrN_6$, C, 54.74; H, 3.06; N, 10.64; found: C, 54.81; H, 3.40; N, 10.64%.

Complex $(ppy)_2Ir(fpptz)$. This complex was prepared according to the procedure used for the synthesis of $(ppy)_2Ir(tfmpptz)$, in a yield of 70%. ^{1}H NMR (600 MHz, DMSO-d_6): δ 8.19–8.15 (3H, m), 8.02 (1H, t), 7.95 (2H, dd), 7.86–7.83 (3H, m), 7.80 (1H, d), 7.64 (1H d), 7.60 (2H, d), 7.35 (1H, t), 7.19–7.12 (4H, m), 6.95 (1H, t), 6.88 (1H, t), 6.85 (1H, t), 6.75 (1H, t), 6.19 (2H, dd). FT-IR (KBr) cm^{-1}: 2029, 1640, 1606, 1586, 1515, 1482, 1424, 1221, 1154, 760, 628. $C_{35}H_{24}FIrN_6$, C, 56.82; H, 3.27; N, 11.36; found: C, 56.90; H, 3.18; N, 11.38%.

Complex $(ppy)_2Ir(tfmptz)$. This complex was prepared according to the procedure used for the synthesis of $(ppy)_2Ir(tfmpptz)$, in a yield of 60%. ^{1}H NMR (600 MHz, DMSO-d_6): δ 8.21–8.17 (3H, m), 8.07 (1H, dt), 7.89–7.84 (3H, m), 7.93 (1H, d), 7.64 (1H, d), 7.58 (1H d), 7.51 (1H, d), 7.45 (1H, dt), 7.21 (1H, dt), 7.13 (1H, dt), 6.96 (1H, dt), 6.89–6.84 (2H, m),6.74 (1H, dt), 6.19 (1H, d), 6.14 (1H, dt), 6.93 (1H, s), 6.88 (1H, dt), 6.86 (1H, dt), 6.61 (1H, s), 6.33 (2H, t), 6.01 (1H, d). FT-IR (KBr) cm^{-1}: 2029, 1635, 1606, 1478, 1204, 1134, 760, 574. $C_{30}H_{20}F_3IrN_6$, C, 50.84; H, 2.82; N, 11.77; found: C, 51.02 H, 3.20; N, 11.67%.

3. Results and discussion

3.1 Single-crystal structures

The X-ray single-crystal structure diffraction studies were carried out to reveal the exact structures of $(ppy)_2Ir(tfmpptz)$, $(ppy)_2Ir(fpptz)$ and $(ppy)_2Ir(tfmptz)$. The crystal structure data are shown in Table 1. These complexes show distorted octahedral geometries with two cyclometalated ppy ligands and one N^N ligand surrounding the iridium metal center, as displayed in Fig. 1. It is obvious that ppy ligands in complexes $(ppy)_2Ir(tfmpptz)$ and $(ppy)_2Ir(fpptz)$ are located in the *trans* orientation, showing the typical coordinated geometries.[22] The coordination pattern of ppy chelates in $(ppy)_2Ir(tfmptz)$ changes into *cis* orientation as shown in Fig. 1c. The associated Ir–N distances on the N^N ligands are significantly shorter than that on ppy ligands because of the stronger electron-withdrawing abilities of triazol. The Ir–N bond lengths between Ir(III) metal and tfmptz for $(ppy)_2(tfmptz)$ (Ir–N5 = 2.031 Å, Ir–N6 = 2.033 Å) are shorter than those of $(ppy)_2Ir(fpptz)$ (Ir–N5 = 2.054 Å, Ir–N6 = 2.038 Å) and

Table 1 Crystallographic data for $(ppy)_2Ir(fpptz)$, $(ppy)_2Ir(tfmpptz)$ and $(ppy)_2Ir(tfmptz)$

	$(ppy)_2Ir(fpptz)$	$(ppy)_2Ir(tfmpptz)$	$(ppy)_2Ir(tfmptz)$
Empirical formula	$C_{35}H_{24}FIrN_6$	$C_{36}H_{24}F_3IrN_6$	$C_{30}H_{20}F_3IrN_6$
Crystal size (mm^3)	0.23 × 0.21 × 0.19	0.19 × 0.14 × 0.09	0.23 × 0.21 × 0.19
Formula weight	739.80	789.81	713.72
Temperature (K)	296(2)	293(2)	293(2)
Wavelength (Å)	0.71073	0.71073	0.71073
Crystal system	Orthorhombic	Triclinic	Triclinic
Space group	*Pbca*	$P\bar{1}$	$P\bar{1}$
a (Å)	13.163(7)	9.979(5)	9.307(7)
b (Å)	20.032(11)	12.906(7)	12.792(9)
c (Å)	23.737(13)	13.397(7)	13.798
α (deg)	90	94.040(5)	96.684(7)
β (deg)	90	94.595(5)	98.707(7)
γ (deg)	90	105.072(5)	109.386(6)
Volume ($Å^3$)	6259(6)	1653.2(15)	1507.1(19)
Z	8	2	2
Reflections collected	35 723/5632 [*R*(int) = 0.0906]	11 818/5861 [*R*(int) = 0.0486]	10 862/5526 [*R*(int) = 0.0406]
Goodness-of-fit on F^2	1.002	1.009	1.026
R indices (all data)	R_1 = 0.0780, wR_2 = 0.0791	R_1 = 0.0543, wR_2 = 0.0815	R_1 = 0.0568, wR_2 = 0.0900

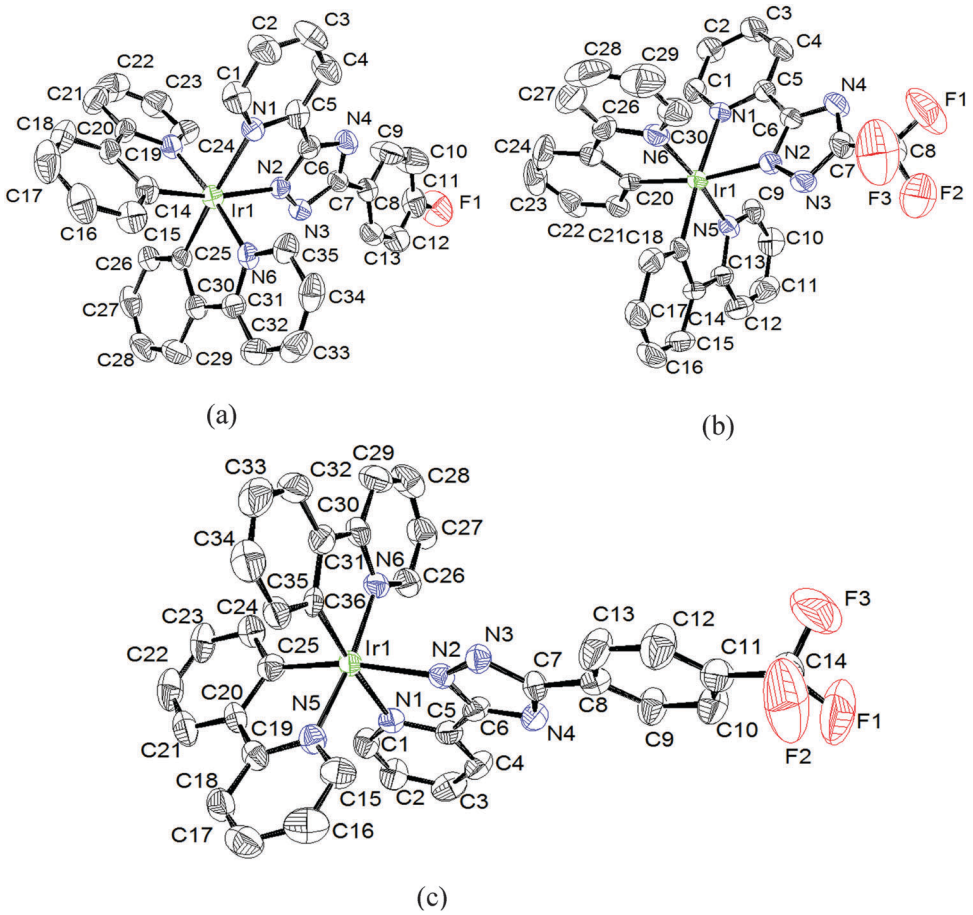

Fig. 1 ORTEP diagrams of $(ppy)_2Ir(fpptz)$ (a), $(ppy)_2Ir(tfmpptz)$ (b) and $(ppy)_2(tfmptz)$ (c) with thermal ellipsoids shown at the 30% probability level. (Selected bond distances and angles for $(ppy)_2Ir(fpptz)$: Ir(1)–N(1) = 2.182(5), Ir(1)–N(2) = 2.133(5), Ir(1)–N(5) = 2.054(5), Ir(1)–N(6) = 2.038(5), Ir(1)–C(14) = 1.999(6), Ir(1)–C(25) = 2.009(6) Å; N(2)–Ir(1)–N(1) = 76.25(19), N(5)–Ir(1)–N(1) = 88.89(19), C(14)–Ir(1)–C(25) = 89.2(2), C(14)–Ir(1)–N(5) = 80.2(2)°. Selected bond distances and angles for $(ppy)_2Ir(tfmpptz)$: Ir(1)–N(1) = 2.175(5), Ir(1)–N(2) = 2.124(5), Ir(1)–N(5) = 2.032(5), Ir(1)–N(6) = 2.042(5) Å, Ir(1)–C(15) = 2.003(6), Ir(1)–C(26) = 2.013(6); N(2)–Ir(1)–N(1) = 76.48(19), N(5)–Ir(1)–N(1) = 89.8(2), C(15)–Ir(1)–C(26) = 89.9(2), C(15)–Ir(1)–N(5) = 80.1(2)°. Selected bond distances and angles for $(ppy)_2(tfmptz)$: Ir(1)–N(1) = 2.165(5), Ir(1)–N(2) = 2.126(5), Ir(1)–N(5) = 2.031(6), Ir(1)–N(6) = 2.033(6), Ir(1)–C(19) = 2.024(7), Ir(1)–C(30) = 2.011(7) Å; N(2)–Ir(1)–N(1) = 76.4(2), N(5)–Ir(1)–N(2) = 92.1(2), C(19)–Ir(1)–C(30) = 87.6(2), N(5)–Ir(1)–N(2) = 92.1(2)°.)

$(ppy)_2Ir(tfmpptz)$ (Ir–N5 = 2.032 Å, Ir–N6 = 2.042 Å) due to the isomerization of two ppy chelates. The phenyl-triazole torsional angle of N3–C7–C8–C13 in $(ppy)_2Ir(tfmpptz)$ is closer to coplanarity (4.4°). While, the phenyl ring twists to the opposite position with respect to the triazole ring with a value of −26.8°.

3.2 Absorption and emission spectra

Fig. 2 shows the UV-vis absorption spectra of complexes $(ppy)_2Ir(tfmpptz)$, $(ppy)_2Ir(fpptz)$ and $(ppy)_2Ir(tfmptz)$ in CH_2Cl_2 solution. The time-dependent DFT (TD-DFT) calculations indicated that the intense absorption bands at 250–270 nm are mainly attributed to the π–π* transition of the triazole ligands and the shoulders at 280–320 nm are due to the transitions centered on the ppy ligand. The weaker absorption bands at around 350–360 nm originated from the spin-allowed singlet-to-singlet metal-to-ligand charge-transfer (^{1}MLCT). The absorption bands at >400 nm, which were amplified and are displayed in the inset, are assigned to mixtures of spin-forbidden singlet-to-triplet ^{3}MLCT and ^{3}LC known for iridium complexes because of the strong spin–orbit coupling.[23] The absorption of the $(ppy)_2Ir(fpptz)$ complex with the larger phenyl-triazole torsional angle has a slight blue shift relative to that of $(ppy)_2Ir(tfmpptz)$.

The optical energy gaps (E_g) of the complexes were calculated according to their absorption edges and are listed in Table 2. E_g of $(ppy)_2Ir(tfmpptz)$, $(ppy)_2Ir(fpptz)$ and $(ppy)_2Ir(tfmptz)$ are 2.61, 2.60 and 2.62 eV, which are larger than that of $Ir(ppy)_3$.[8] Complexes $(ppy)_2Ir(tfmpptz)$ and $(ppy)_2Ir(fpptz)$ show smaller E_g than $(ppy)_2Ir(tfmptz)$, which is due to the increased conjugation.

The titled complexes exhibit the bright blue-green emission at room temperature in CH_2Cl_2 solution and the emission spectrum of $Ir(ppy)_3$ was also recorded under the same conditions, as shown in Fig. 3. The emission spectra of the $(ppy)_2Ir(N^\wedge N)$ complex have the similar profiles with the intense peaks at around 485 nm and a shoulder near 513 nm. The vibronic structure of the emission bands indicates a large amount of ^{3}LC character. The peaks at around 485 nm may originate from the N^N ligands. Meanwhile, the emission shoulder at 513 nm is consistent with the maximum emission peak of $Ir(ppy)_3$, which is due to the ^{3}MLCT and ^{3}LC states centered on the ppy ligands.[24] The order of the maximum peaks at emission spectra is $(ppy)_2Ir(tfmptz)$ < $(ppy)_2Ir(tfmpptz)$ < $(ppy)_2Ir(fpptz)$ < $Ir(ppy)_3$. This emission behavior was attributed to the increasing electron-withdrawing abilities of the ligands along the same order.[15] The poor overlap between the emission and absorption bands is due to the origin of emission possessing excessive ligand-centered ππ* and relatively low MLCT character.

The photoluminescence quantum yields (PLQY) of $(ppy)_2Ir(tfmpptz)$, $(ppy)_2Ir(tfmptz)$ and $(ppy)_2Ir(fpptz)$ are 60, 47 and 44%, respectively. The $(ppy)_2Ir(tfmpptz)$ complex has a higher

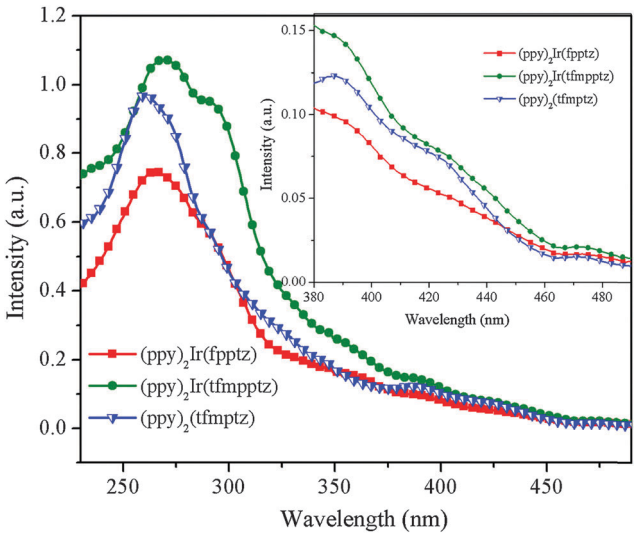

Fig. 2 The absorption spectra of complexes $(ppy)_2Ir(fpptz)$, $(ppy)_2Ir(tfmpptz)$ and $(ppy)_2Ir(tfmptz)$ in CH_2Cl_2 solution. The T_1 absorption transitions are shown in the inset.

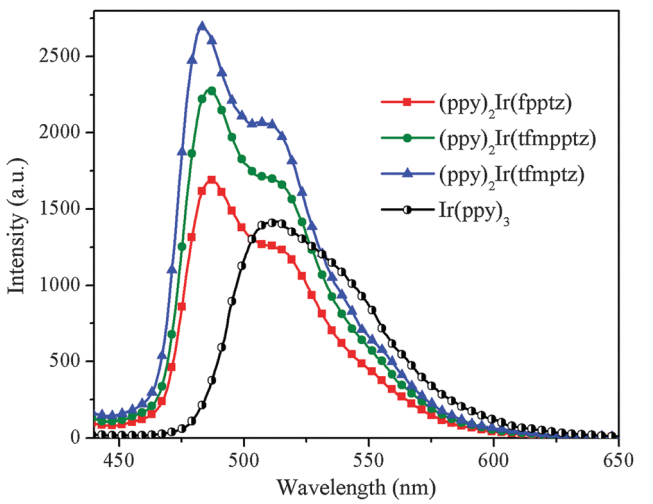

Fig. 3 The emission spectra of complexes $(ppy)_2Ir(N^\wedge N)$ and $Ir(ppy)_3$ in CH_2Cl_2 solution at room temperature.

Table 2 Absorption and emission data, HOMO and LUMO levels, and optical bandgap (E_g) and quantum yields (Φ) in CH_2Cl_2 solution of all titled complexes

Complexes	λ_{abs} (nm)	$\lambda_{max,em}$ (nm)	HOMO[a] (eV)	LUMO[b] (eV)	E_g[c] (eV)	Φ (%)
$(ppy)_2Ir(tfmpptz)$	269, 292, 355, 387, 426, 474	485, 513	−5.64	−3.03	2.61	60
$(ppy)_2Ir(fpptz)$	264, 284, 348, 389, 425, 475	487, 516	−5.78	−3.20	2.60	44
$(ppy)_2Ir(tfmptz)$	250, 298, 351, 387, 424, 474	483, 510			2.62	47
$Ir(ppy)_3$		510	−5.3	−2.9	2.4	

[a] HOMO = eE_{ox} − 4.74, E_{ox} obtained from cyclic voltammetry. [b] LUMO = HOMO − E_g.[25] [c] E_g obtained from the onset of UV-vis absorption spectra.

quantum yield (Φ) than others because of the better coplanarity and the increased conjugation.

3.3 Electrochemical properties

The electrochemical behaviors of all complexes were examined by cyclic voltammetry and the values of E_{HOMO} (HOMO: the highest occupied molecular orbital) and E_{LUMO} were obtained according to the equation $E_{LUMO} = E_g - E_{HOMO}$ and are also listed in Table 2. The HOMO/LUMO levels of $(ppy)_2Ir(tfmpptz)$ and $(ppy)_2Ir(fpptz)$ are −5.64/−3.03 and −5.78/−3.20 eV. It is noticeable that the introduction of an ancillary ligand can make the HOMO and LUMO stabilize relative to $Ir(ppy)_3$ (the HOMO/LUMO levels of $Ir(ppy)_3$ are −2.9/−5.3 eV[26]). These lower LUMO levels benefit the electron injection from the cathode in the devices.

In order to investigate the photophysical properties of the compounds, DFT was applied to molecular orbital studies. The results indicated that complexes $(ppy)_2Ir(tfmpptz)$, $(ppy)_2Ir(fpptz)$ and $(ppy)_2Ir(tfmptz)$ have the similar frontier molecular orbitals. Taking $(ppy)_2Ir(tfmpptz)$ for example as shown in Fig. 4, the HOMOs are absolutely dominated by the Ir^{3+} cores involving the contributions of the Ir d-orbitals and the π-orbitals attributed to the phenyls of ppy and 1,2,4-triazole, and the LUMOs are largely located at the π* orbital from ppy and pyridine of tfmpptz. One of the ppy and 4-(trifluoromethyl)phenyl moieties has no contribution to LUMO and LUMO+1.

3.4 Electroluminescence characterization

The electroluminescence properties of the complexes were examined by doping them into the host as emitting layers. The structures of devices A–C are ITO/NPB (40 nm)/CBP: $(ppy)_2Ir(N^\wedge N)$ (6 wt%, 30 nm)/TPBi (35 nm)/LiF(1 nm)/Al (200 nm). The $(ppy)_2Ir(N^\wedge N)$ complex consists of $(ppy)_2Ir(fpptz)$ (device A), $(ppy)_2Ir(tfmpptz)$ (device B), and $(ppy)_2Ir(tfmptz)$ (device C). Normalized EL spectra peaks of devices A–C appear at 490 nm and a shoulder peak at around 516–519 nm, as displayed in Fig. 5. The spectral features and emission energies in EL spectra resemble those in PL spectra very closely, indicating that the emission originates from the same species in both EL and PL spectra. The emissions of NPB and CBP were not observed, suggesting that the complete energy transfer occurs from CBP to the $(ppy)_2Ir(N^\wedge N)$ complex.

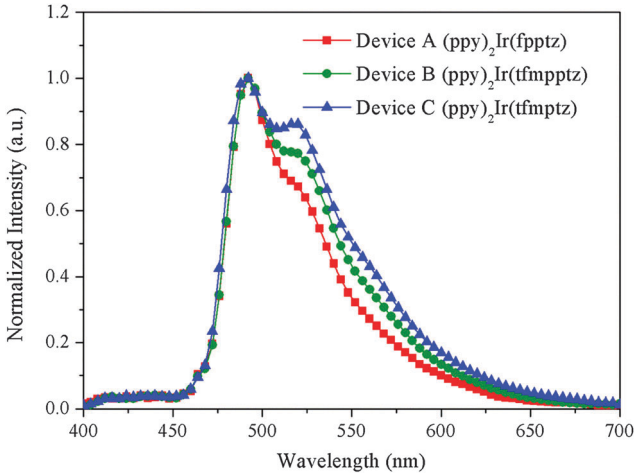

Fig. 5 The EL spectra of devices A–C at a voltage of 5 V.

Devices A–C show the maximum luminance (L_{max}) of 7724 cd m^{-2} at a voltage of 6 V, 7261 cd m^{-2} at a voltage of 5.7 V and 5114 cd m^{-2} at a voltage of 5.7 V, respectively, as displayed in Fig. 6a. The lower turn-on voltages (the voltage at a brightness of 1 cd m^{-2}) were 3.3, 3.2 and 3.0 V, as listed in Table 3. Devices A and B have the similar performances based on the $(ppy)_2Ir(fpptz)$ and $(ppy)_2Ir(tfmpptz)$ complexes with the same current and power efficiency (η_c = 4.1 cd A^{-1} and η_p = 3.2 lm W^{-1}) as shown in Fig. 6b. The $(ppy)_2Ir(tfmptz)$ complex (device C) exhibits better performances with higher current efficiency (η_c = 4.5 cd A^{-1}) and higher power efficiency (η_p = 3.7 lm W^{-1}). But devices A and B exhibit the lower roll-off efficiency, which is attributed to the increased conjugation due to the phenyl group of complexes $(ppy)_2Ir(fpptz)$ and $(ppy)_2Ir(tfmpptz)$. Compared with device B, device A has the lower roll-off efficiency because the larger torsional angle between the triazole and the phenyl ring results in a larger steric hindrance. Consequently, triplet–triplet annihilation can be weakened.

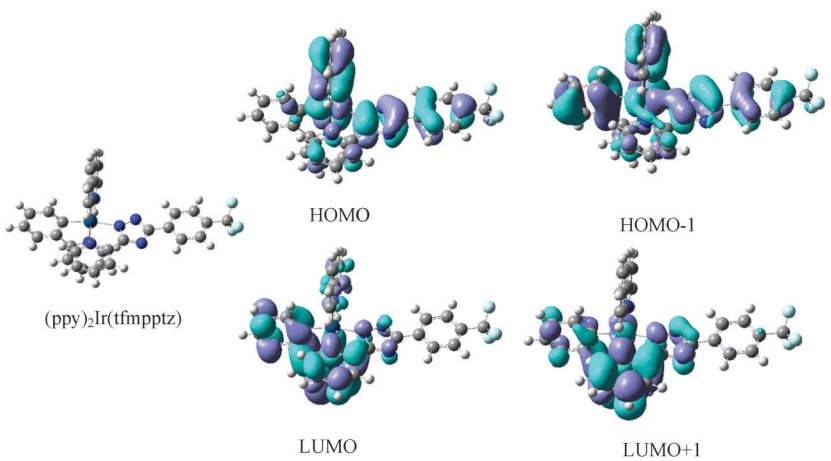

Fig. 4 Optimized molecular structure and frontier molecular orbitals characterization of $(ppy)_2Ir(tfmpptz)$.

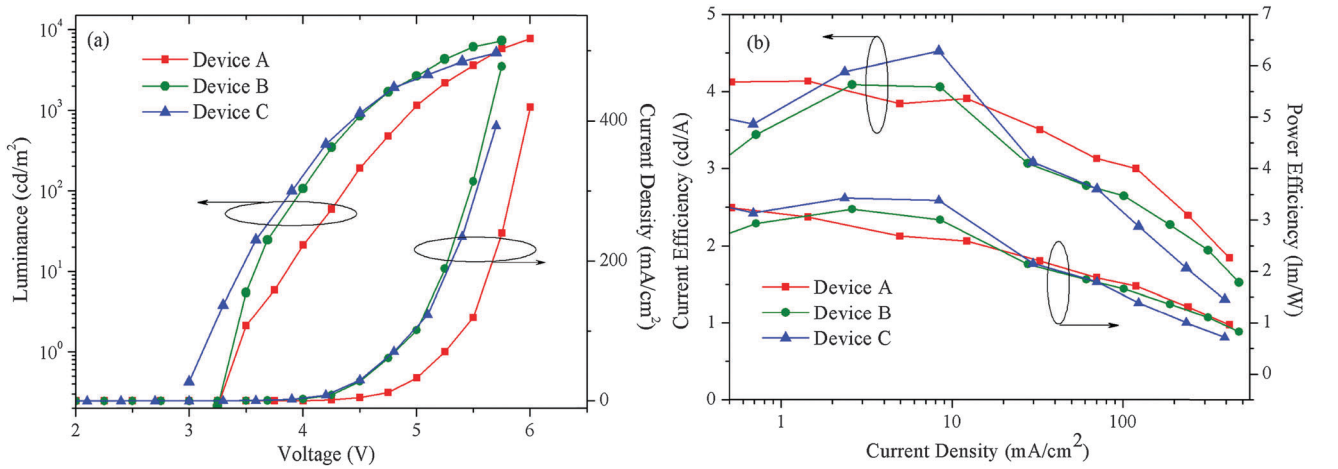

Fig. 6 The L–V–J (a) and η_c–J–η_p (b) curves of devices A–C.

Table 3 The performances of devices A–C

Device	V_{on}[a] (V)	L_{max}[b] (cd m^{-2})	η_c[c] (cd A^{-1})	η_p[d] (lm W^{-1})	λ_{max}[e] (nm)
A	3.3	7724	4.1	3.2	491, 519
B	3.2	7261	4.1	3.2	490, 518
C	3.0	5114	4.5	3.7	490, 515

[a] The voltage at a brightness of 1 cd m^{-2}. [b] The maximum luminance. [c] The maximum current efficiency. [d] The maximum power efficiency. [e] The peaks of EL spectra.

4. Conclusions

The molecular structures, and photophysical, electrochemical and electroluminescence properties of four (ppy)$_2$Ir(N^N) complexes have been investigated. These complexes exhibit wider optical energy gaps than those of tris (2-phenylpyridine) iridium. Their PL and EL spectra are located in the blue-green light range. The devices were fabricated by using (ppy)$_2$Ir(N^N) complexes as guests in order to characterize the electroluminescence properties. The device employing (ppy)$_2$Ir(tfmpptz) doped in CBP as a light-emitting layer had a better performance. The relationships between the molecular structure and photoelectric performances were discussed in detail.

Acknowledgements

This work was financially supported by the International Science and Technology Cooperation Program of China (2012DFR50460); the National Natural Scientific Foundation of China (21071108, 60976018, 21101111, 61274056 and 61205179); the Natural Science Foundation of Shanxi Province (2011021022-2 and 2010021023-2); the Program for Changjiang Scholar and Innovation Research Team in University (IRT0972); and the Key Scientific and Technological Project of Shanxi Province (20120321019).

References

1 Y. M. Jin, C. C. Wang, L. S. Xue, T. Y. Li, S. Zhang, X. Liu, X. Liang, Y. X. Zheng and J. L. Zuo, *J. Organomet. Chem.*, 2014, **765**, 39–45.
2 W.-Y. Wong and C.-L. Ho, *J. Mater. Chem.*, 2009, **19**, 4457–4482.
3 E. Orselli, J. Maunoury, D. Bascour and J. P. Catinat, *Org. Electron.*, 2012, **13**, 1506–1510.
4 W.-Y. Wong and C.-L. Ho, *Coord. Chem. Rev.*, 2009, **253**, 1709–1758.
5 L. Ying, C.-L. Ho, H. Wu, Y. Cao and W.-Y. Wong, *Adv. Mater.*, 2014, **26**, 2459–2473.
6 X. Yang, G.-J. Zhou and W.-Y. Wong, *J. Mater. Chem. C*, 2014, **2**, 1760–1778.
7 G. G. Shan, H. B. Li, H. T. Cao, D. X. Zhu, Z. M. Su and Y. Liao, *J. Organomet. Chem.*, 2012, **713**, 20–26.
8 M. C. Suh, H. Y. Shin and S. J. Cha, *Org. Electron.*, 2013, **14**, 2198–2203.
9 L. C. Chen, Z. H. Ma, J. Q. Ding, L. X. Wang, X. B. Jing and F. S. Wang, *Org. Electron.*, 2012, **13**, 2160–2166.
10 S. J. Lee, J. S. Park, M. Song, I. A. Shin, Y. I. Kim, J. W. Lee, J. W. Kang, Y. S. Gal, S. Kang, J. Y. Lee, S. H. Jung, H. S. Kim, M. Y. Chae and S. H. Jin, *Adv. Funct. Mater.*, 2009, **19**, 2205–2212.
11 K. Y. Lu, H. H. Chou, C. H. Hsieh, Y. H. Yang, H. R. Tsai, H. Y. Tsai, L. C. Hsu, C. Y. Chen, I. C. Chen and C. H. Cheng, *Adv. Mater.*, 2011, **23**, 4933–4937.
12 C.-L. Ho and W.-Y. Wong, *New J. Chem.*, 2013, **37**, 1665–1680.
13 G.-J. Zhou, C.-L. Ho, W.-Y. Wong, Q. Wang, D. Ma, L. Wang, Z. Lin, T. B. Marder and A. Beeby, *Adv. Funct. Mater.*, 2008, **18**, 499–511.
14 C.-L. Ho, Q. Wang, C. S. Lam, W.-Y. Wong, D. Ma, L. Wang, Z. Q. Gao, C. H. Chen, K. W. Cheah and Z. Lin, *Chem. – Asian J.*, 2009, **4**, 89–103.
15 H. X. Xu, Y. Yue, L. T. Qu, Y. Y. Hao, H. Wang, L. Q. Chen and B. S. Xu, *Dyes Pigm.*, 2013, **99**, 67–73.
16 X. Zhang, C. Jiang, Y. Mo, Y. Xu, H. Shi and Y. Cao, *Appl. Phys. Lett.*, 2006, **88**, 051116.
17 F. Dumur, M. Lepeltier, B. Graff, E. Contal, G. Wantz, J. Lalevée, C. R. Mayer, D. Bertin and D. Gigmes, *Synth. Met.*, 2013, **182**, 13–21.
18 B. Chen, Y. Li, W. Yang, W. Luo and H. Wu, *Org. Electron.*, 2011, **12**, 766–773.

19 A. D. Becke, *Phys. Rev. A*, 1988, **38**, 3098–3100.
20 C. Lee, W. T. Yang and R. G. Parr, *Phys. Rev. B: Condens. Matter Mater. Phys.*, 1988, **37**, 785–789.
21 E. Baranoff, B. F. E. Curchod, F. Monti, F. Steimer, G. Accorsi, I. Tavernelli, U. Rothlisberger, R. Scopelliti, M. Gratzel and M. K. Nazeeruddin, *Inorg. Chem.*, 2012, **51**, 799–811.
22 V. K. Rai, M. Nishiura, M. Takimoto, S. S. Zhao, Y. Liu and Z. M. Hou, *Inorg. Chem.*, 2012, **51**, 822–835.
23 E. Orselli, G. S. Kottas, A. E. Konradsson, P. Coppo, R. Fröhlich, L. De Cola, A. Dijken, M. Büchel and H. Börner, *Inorg. Chem.*, 2007, **46**, 11082–11093.
24 G.-J. Zhou, W.-Y. Wong and X. Yang, *Chem. – Asian J.*, 2011, **6**, 1706–1727.
25 W. Lee, T.-H. Kwon, J. Kwon, J.-Y. Kim, C. Lee and J.-I. Hong, *New J. Chem.*, 2011, **35**, 2557–2563.
26 Y. J. Cho, K. R. Wee, H. J. Son, D. W. Cho and S. O. Kang, *Phys. Chem. Chem. Phys.*, 2014, **16**, 4510–4521.